IEEE Photonics Journal
An IEEE Photonics Society Publication

Open Access

A Novel Manipulation for Implementing Logic Operations Based on Plasmonic Resonators

Volume 11, Number 1, February 2019

Junxiong Chai
Yiyuan Xie
Yichen Ye
Lixia Fu
Lili Li
Ye Su
Ying Xiao
Yong Liu

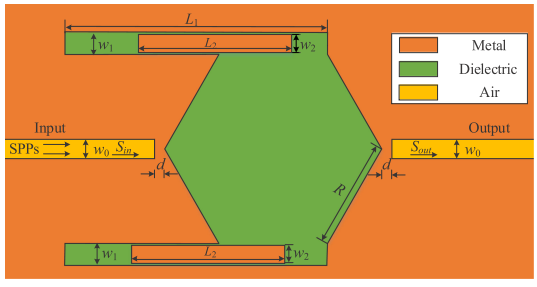

DOI: 10.1109/JPHOT.2019.2892994
1943-0655

A Novel Manipulation for Implementing Logic Operations Based on Plasmonic Resonators

Junxiong Chai,[1] Yiyuan Xie,[1,2,3] Yichen Ye,[1] Lixia Fu,[1] Lili Li,[1] Ye Su,[1] Ying Xiao,[1] and Yong Liu[3]

[1]School of Electronics and Information Engineering, Southwest University, Chongqing 400715, China
[2]Chongqing Key Laboratory of Nonlinear Circuits and Intelligent Information Processing, Chongqing 400715, China
[3]School of Optoelectronic Information, University of Electronic Science and Technology of Chengdu, Sichuan 611731, China

DOI:10.1109/JPHOT.2019.2892994

Manuscript received December 9, 2018; revised January 8, 2019; accepted January 10, 2019. Date of publication January 14, 2019; date of current version February 7, 2019. This work was supported in part by the 863 program of China under Grant 2015AA016304, in part by the National Natural Science Foundation of Chongqing City under Grant Nos. cstc2016jcyjA2002, in part by the Postdoctoral Science Foundation of China under Grant Nos. 2016M590875, and in part by the Fundamental Research Funds for the Central Universities under Grant XDJK2018B012. Corresponding author: Yiyuan Xie. (e-mail: yyxie@swu.edu.cn).

Abstract: In this paper, a plasmonic logic device with the novel manipulation method is proposed. It consists of a hexagonal resonator in the center of the structure and dual rectangular resonators in which two sliders are embedded. The input states of the logic gate are represented by the positions of the slider. The temporal coupled-mode theory demonstrates that different positions of the slider lead to changes in the transmission spectra, which is the main idea in achieving logic operation. Ultimately, three logic operations (AND, XOR, and NOR) can be implemented simultaneously by moving the sliders and the finite-difference time-domain method is used for numerical validation. In addition, the influence of structural parameters on transmission characteristics and contrast ratio is also investigated. This paper is of great significance to the design of optical logic device on-chip and provides a new method for designing other integrated photonic devices.

Index Terms: Logic gate, resonators, surface plasmon polaritons (SPPs), transmission characteristics.

1. Introduction

Surface plasmon polaritons (SPPs) are the electromagnetic waves that are formed by the interaction between free electrons and electromagnetic field on the metal surface and propagate along the surface of the metal-dielectric [1]–[4]. They are exponentially attenuated in the vertical direction and are expected to break the classical diffraction limit [5]–[7]. In order to manipulate light in nanoscale domain, many kinds of plasmonic waveguides have been proposed for propagating SPPs, such as nanowires, v-shaped hybrid plasmonic waveguides, dielectric-loaded waveguides and metal-insulator-metal (MIM) waveguides [8], [9]. The MIM waveguides received extensive attention in recent years since they have the advantages of strong confinement to SPPs, easy manufacturing

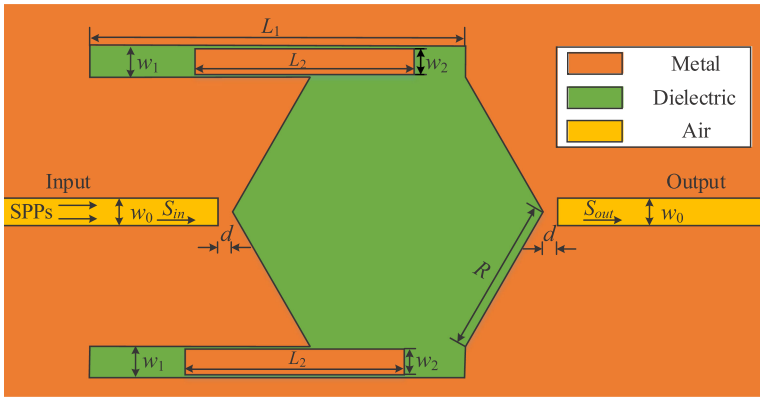

Fig. 1. Schematic diagram of the proposed plasmonic logic device.

and acceptable propagation length [10]–[12]. various optical nanoscale devices based on MIM waveguides have been proposed, including filters [13], [14], demultiplexers [15], [16], sensors [17], [18], switches [19], [20], splitters [21], [22] and logic gates [23]–[29]. Among these devices, logic gate, as a essential component of optical computing and all-optical information processing, plays an important role in the research of optical communication. Therefore, the optical logic gate has become a current research hotspot and has been extensively studied by a large number of scholars.

Currently, there are two main ways to design logic gates. The first method is linear interference whose basic idea is the constructive or destructive interference between two input signals [23]–[25]. Predecessors made outstanding contributions in terms of logic gates based on this approach. However, for linear interference, it is difficult to precisely control the phase difference of the input signals, which may cause instability of the output signal [26]. In order to avoid the above problem, researchers proposed many logic devices based on nonlinear processes, such as third-order nonlinear effects. The nonlinear Kerr effect was utilized to implement logic operations [27]. A multifunctional logic gate was realized by setting optical pulse to different intensities based on nonlinear plasmonic resonator [28]. Although the plasmonic devices proposed have great performance and can implement a plurality of logic operations in the same structure, most of them cannot implement multiple logic operations simultaneously. As we all know, the logic device that can implement multiple logic operations at the same time has higher computing speed and integration which are urgently needed for on-chip optical signal processing. However, to our best knowledge, this kind of promising logic device is still rare.

To meet these demands, a logic device with a novel manipulation method, the position of the slider represents the Boolean value of the input signal, is investigated in this paper. The different positions of the sliders result in diverse effective paths for the resonator and eventually cause a variation of the transmission spectra. By monitoring the transmission of the output signal at different wavelengths, three logic operations (AND, XOR, and NOR) can be simultaneously achieved in the same structure. The contrast ratio for the AND, XOR and NOR logic gates are 19 dB, 16 dB and 21 dB, respectively, which are higher than similarly plasmonic logic devices [23], [27], [29]. In addition, we further investigate the influence of structural parameters on the transmission characteristics and contrast ratio of logic gates. This novel method can be used for designing other optical nanoscale devices.

2. Structure Model and Theoretical Analysis

A two-dimensional schematic diagram of the proposed plasmonic structure is shown in the Fig. 1. The two rectangular resonators are respectively tangent to the hexagonal resonator. The structure proposed can be realized by using the nanoimprint lithography (NIL) technology with a resolution of sub-4 nm or less [30]–[32]. The dimensional parameters of the structure R, L_1 and L_2 are

the side length of the hexagonal resonator, the length of the rectangular resonators and sliders severally. w_0, w_1 and w_2 are the width of the MIM waveguides, rectangular resonators and sliders. d denotes the coupling distance between the boundary of the hexagonal resonator and the MIM waveguides. In the structure, the medium of waveguides is set to be air. The refractive index of dielectric embedded in the cavity is n. The metal is assumed as silver, whose complex relative permittivity can be characterized by the well-known Drude model [2]:

$$\varepsilon_m(\omega) = \varepsilon_\infty - \omega_p^2/[\omega(\omega + i\gamma)] \tag{1}$$

where $\varepsilon_\infty = 3.7$, $\omega_p = 9.1$ eV, and $\gamma = 0.018$ eV respectively represent the dielectric constant of the infinite frequency, the bulk plasma frequency and the electron collision frequency. ω represents the angular frequency of the incident wave. In this model, since the width w_0 is much smaller than the wavelength of the incident light, only the fundamental TM waveguide mode can propagate whose dispersion relation in the MIM waveguides can be obtained by the following equation [33]:

$$(\varepsilon_m k_d) \tanh\left(\frac{w k_d}{2}\right) + \varepsilon_d k_m = 0 \tag{2}$$

$$k_{d,m} = \sqrt{\beta^2 - \varepsilon_{d,m} k_0^2} \tag{3}$$

where ε_d and ε_m are the permittivities, and $k_{d,m}$ are the propagation constants in the dielectric and metal. $\beta = k_0 n_{eff}$ stands for the wave vector in the MIM waveguides and $k_0 = 2\pi/\lambda$ means the wave vector in vacuum. n_{eff} represents the effective refractive index in the MIM waveguides.

The SPPs propagate along MIM waveguide and will be coupled into the resonator. According to the temporal coupled-mode theory, transmission characteristics of the structure can be investigated. The temporal evolution of normalized amplitude A of the hexagonal resonator can be described as [16]:

$$\frac{dA}{dt} = (j\omega_o - k_o - k_e)A + e^{j\theta}\sqrt{k_e}S_{\text{in}} \tag{4}$$

where ω_o is the resonance frequency of the resonator, k_o, k_e, θ stand for the decay rate of the field induced by the internal loss in the nanocavity, the power coupled into the waveguide and the phase difference that occurs when SPPs are coupled from the waveguide to the cavity, respectively. When amplitude S_{in} of the input signal has an $e^{j\omega t}$ dependence on time and $d_A/d_t = j\omega_o$, A is derived as:

$$A = \frac{e^{j\theta}\sqrt{k_e}S_{\text{in}}}{j(\omega - \omega_o) + k_o + k_e} \tag{5}$$

According to the conservation of energy, we can get the amplitude S_{out} of the output signal as:

$$S_{\text{out}} = e^{-j\theta}\sqrt{k_e}A \tag{6}$$

The transmission efficiency T of the structure can be obtained based on the above equations:

$$T = \left|\frac{S_{\text{out}}}{S_{\text{in}}}\right|^2 = \frac{k_e^2}{(\omega - \omega_o)^2 + (k_o + k_e)^2} \tag{7}$$

When the input signal frequency ω is equal to the resonance frequency ω_o, the transmission achieve a maximum value T_{max}, and the maximum value is:

$$T_{\text{max}} = \frac{k_e^2}{(k_o + k_e)^2} \tag{8}$$

For this SPPs cavity, the resonance condition can be given by [16]:

$$2m\pi = \frac{2\pi(6R + L')R_e(N_{eff})}{\lambda_m} + \phi \tag{9}$$

where λ_m is the resonance wavelength, N_{eff} is the effective index in the cavity for SPPs that is dependent on the refractive index n of dielectric, m is a positive integr corresponding to the number

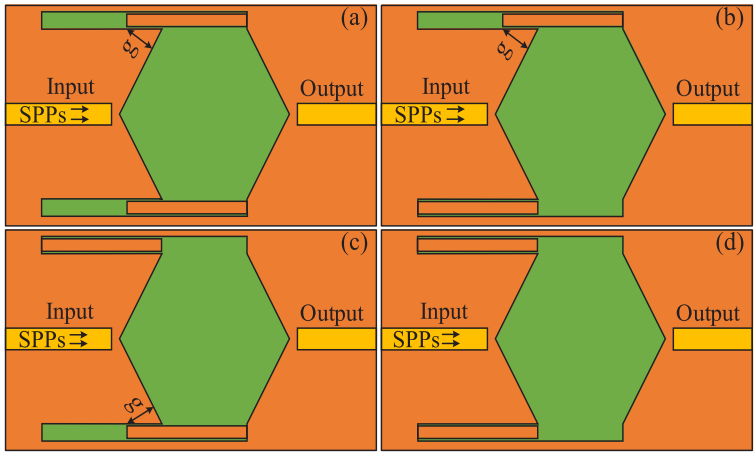

Fig. 2. The schematic diagram when the input state is (a) (X = 1, Y = 1), (b) (X = 1, Y = 0), (c) (X = 0, Y = 1), (d) (X = 0, Y = 0).

of standing waves in the cavity, and ϕ represents the total phase shift at the corners of the cavity. L' is the additional length due to the slider movement related to the width of the rectangular resonator. From equation (9), it is apparent that the resonance wavelength is related to the refractive index of dielectric and the circumference of the cavity.

3. Results and Discussions

The FDTD method with perfectly matched layer (PML) as boundary conditions is introduced to investigate the transmission characteristics of the structure. And the fundamental TM mode of the MIM waveguide is excited by a mode source. The parameters of structure are set as $L_1 = 700$ nm, $L_2 = 400$ nm, $R = 300$ nm, $w_0 = 50$ nm, $w_1 = 50$ nm, $w_2 = 45$ nm and $d = 15$ nm. The dielectric in the cavity is set to air. The two input Boolean ports of the logic gate are X and Y respectively. When the slider in the upper rectangular resonator is moved to the right, it represents X = 1, whereas it is moved to the left, it represents X = 0. Similarly, the location of the slider in the lower rectangular resonator also represents the different input states of Y. As illustrated in Fig. 2, it shows a schematic diagram of the input states of (X = 1, Y = 1), (X = 1, Y = 0), (X = 0, Y = 1), and (X = 0, Y = 0). Various actuation mechanisms provide the possibility to manipulate the slider, including electrostatic, electromagnetic, and electrothermal [34]. Especially, the design, simulation, optimization and fabrication of electrothermal actuators have been investigated by a large number of scholars [35]–[37]. Therefore, the slider could be attached to one end of the expansion beam, and the heating laser is used to act on the expansion arm. Eventually, the manipulation of the slider is achieved by the expansion and contraction of the expansion arm.

Due to g is larger than the field skin depth in metal [38], it avoids the interaction between the hexagonal resonator and the left end of the rectangular resonator when the slider moves to the right of the rectangular resonator. As can be observed from Fig. 2 that the perimeter of the cavity are different under four input states. Different circumferences of cavity eventually lead to the difference of the transmission spectra, as drawn in Fig. 3. When the input states are (X = 1, Y = 0) and (X = 0, Y = 1), since the structure is symmetrical, the transmission spectra in the two input states are the same as shown by the blue line in the Fig. 3. The transmission spectra of the input states (X = 1, Y = 1), (X = 1, Y = 0 or X = 0, Y = 1) and (X = 0, Y = 0) respectively reach maximum values at the 687.7 nm, 726.7 nm and 779.5 nm. The transmission of the corresponding three wavelengths under four input states are shown in Table 1. By monitoring the transmission value of the output spectra at 687.7 nm, 726.7 nm, and 779.5 nm, three logic functions (AND, XOR, and NOR) can be simultaneously realized at different wavelengths. For three logic operations, when the

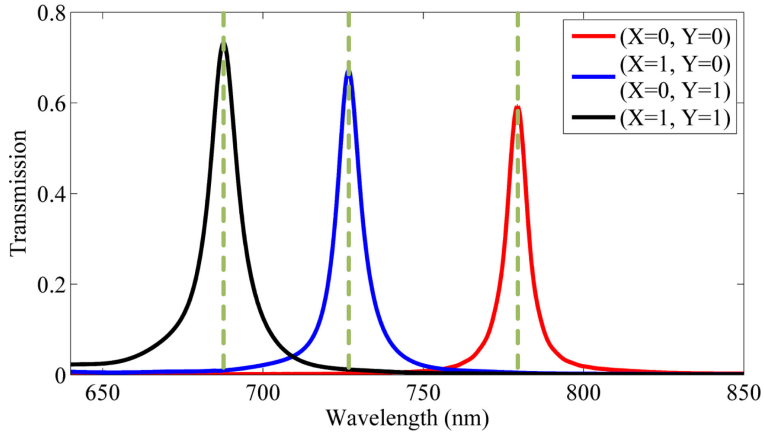

Fig. 3. The transmission spectra of the proposed device under four input states.

TABLE 1
Transmission of Different Input States at Three Wavelengths

Input Logic State		Transmission		
X	Y	687.7nm	726.7nm	779.5nm
1	1	73.2%	1.717%	0.22%
1	0	0.986%	67.2%	0.488%
0	1	0.986%	67.2%	0.488%
0	0	0.136%	0.297%	59.3%

TABLE 2
The Truth Table of AND,XOR and NOR Logic Operations

Input Logic State		Out Logic State		
X	Y	X AND Y	X XOR Y	X NOR Y
1	1	1	0	0
1	0	0	1	0
0	1	0	1	0
0	0	0	0	1

input states meet the corresponding logic relationship, the transmission exceeds 59%. Otherwise, the transmission is lower than 1.8%, as illustrated in Table 1. Therefore, high crosstalk isolation is achieved at output port. Table 2 depicts the truth table of the three logic operations. The detailed implementation process can be explained as follows.

Logic AND operation can be realized by monitoring the transmission at 687.7 nm. When the input state is (X = 1, Y = 1), the transmission reaches the maximum value at 687.7 nm, and the maximum value is 73.2% (logic state 1). However, when the input state is (X = 1, Y = 0) or (X = 0, Y = 1), the transmission at 687.7 nm is 0.986% (logic state 0). And when the input state is (X = 0,

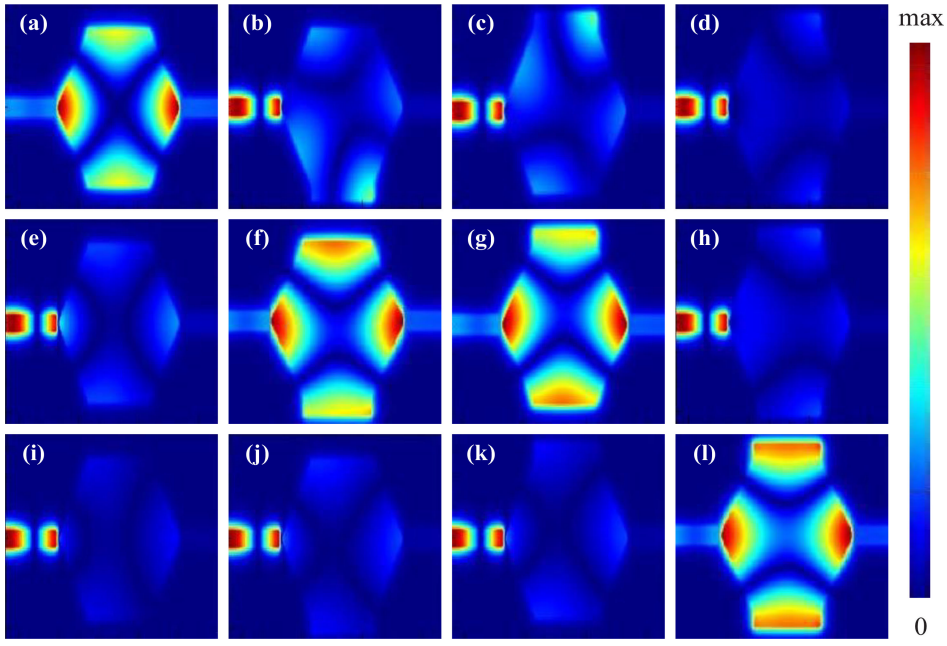

Fig. 4. Field distributions of $|H_Z|$ with the incident light wavelength of 687.7 nm when input state is (a) (X = 1, Y = 1), (b) (X = 1, Y = 0), (c) (X = 0, Y = 1), (d) (X = 0, Y = 0). Field distributions of $|H_Z|$ with the incident light wavelength of 726.7 nm when input state is (e) (X = 1, Y = 1), (f) (X = 1, Y = 0), (g) (X = 0, Y = 1), (h) (X = 0, Y = 0). Field distributions of $|H_Z|$ with the incident light wavelength of 779.5 nm when input state is (i) (X = 1, Y = 1), (j) (X = 1, Y = 0), (k) (X = 0, Y = 1), (l) (X = 0, Y = 0).

Y = 0), the transmission at 687.7 nm is 0.136% (logic state 0). So the proposed logic device can be used as AND logic gate. In addition, the contrast ratio as an important indicator for logic gates between the 1 and 0 states is defined as [39]:

$$\text{Contrast Ratio} = 10 \log \frac{P_{\text{out}|1}}{P_{\text{out}|0}} \tag{10}$$

where $P_{\text{out}|1}$ and $P_{\text{out}|0}$ are the output power at high and low logic states, respectively. According to equation (10), when using the proposed structure to achieve logic AND operation, the contrast ratio is 19 dB. The field distributions of $|H_Z|$ for incident wavelength of 687.7 nm in the four input states are shown in Figs. 4(a)–4(d). It can be seen that the intensity of the field within the cavity is strong when the input state is (X = 1, Y = 1). In other input states, the intensity of the field inside the cavity is weak, so little energy passes through the cavity to the output port.

The process of implementing XOR operation can also be analysed in this way. When the input state is (X = 1, Y = 0) or (X = 0, Y = 1), the transmission spectrum has a maximum value of 67.2% (logic state 1) at 726.7 nm. At this time, when the input state are (X = 1, Y = 1) and (X = 0, Y = 0), the corresponding transmission are 1.717% (logic state 0) and 0.297% (logic state 0). So it can be used as a XOR logic gate and its contrast ratio is 16 dB. Figs. 4(e)–4(h) shows the corresponding field distributions of $|H_Z|$ for incident wavelength of 726.7 nm.

Similarly, when the input state is (X = 0, Y = 0), the maximum transmission is located at 779.5 nm, and the maximum value is 59.3% (logic state 1). At 779.5 nm, the transmission of input state (X = 1, Y = 1) is 0.22% (logic state 0), and the transmission of input state (X = 1, Y = 0 or X = 0, Y = 1) is 0.488% (logic state 0). Therefore, the logic NOR operation is achieved, and the contrast ratio is 21 dB. The corresponding field distributions of $|H_Z|$ for incident wavelength of 779.5 nm are drawn in Figs. 4(i)–4(l).

In order to further research on the proposed logic device, we discuss the influence of structural parameters on the transmission characteristics and contrast ratio. Obviously, the full width at half

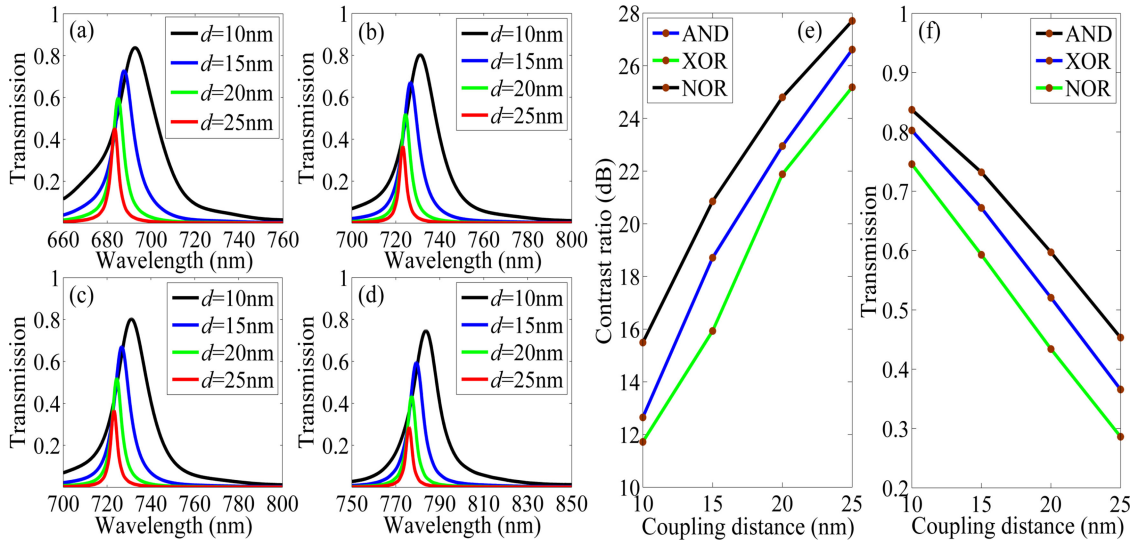

Fig. 5. Transmission spectra of the structure for different coupling distances in (a) (X = 1, Y = 1), (b) (X = 1, Y = 0), (c) (X = 0, Y = 1) and (d) (X = 0, Y = 0) states. (e) The relationship between the contrast ratio of the three logic operations and the coupling distance. (f) The relationship between the transmission of the three logical operations and the coupling distance.

maximum (FWHM) of the transmission spectra in different resonance modes have a significant influence on the contrast ratio. Through equation (8), we can obtain the expression of the FWHM approximately as $4\pi c(k_o + k_e)/\omega_0^2$. Therefore, the FWHM of the resonance spectra can be tuned by controlling the coupling distance. Next, the effect of coupling distance on transmission spectra is studied by simulations. The coupling distance d increases from 10 nm to 25 nm with the step size is 5 nm while the other parameters are fixed. Figs. 5(a)–5(d) illustrates the variation of the transmission spectra for different coupling distance in four input states. As the coupling distance increases, both the transmission and the FWHM of the spectra decrease. Taking into account that these variation may eventually lead to changes in the contrast ratio which is an indicator to evaluate the performance of logic gates. Therefore, the relationship between the contrast ratio of the three logic operations and the coupling distance is plotted in Fig. 5(e). It can be seen that the contrast ratio of the logic gate increases as the coupling distance increases. However, the transmission of the three logic gates will decrease as shown in Fig. 5(f). Therefore, this is a trade-off problem. In order to achieve higher transmission and suitable contrast ratio, the coupling distance is set to 15 nm in this paper.

Moreover, the effect of the width of rectangular resonator on resonance wavelength is investigated. We take $R = 300$ nm, $L_1 = 700$ nm, $d = 15$ nm, $w_0 = 50$ nm, $w_2 = w_1 - a$ and $a = 5$ nm. The width of the rectangular resonator w_1 increases from 50 nm to 65 nm with an interval of 5 nm. The relationship between the width of the rectangular resonator and the resonance wavelength in the four input states is shown in Fig. 6. We can observe that with the increase of the width of the rectangular resonator, the resonance wavelengths of the input states (X = 1, Y = 0), (X = 0, Y = 1) and (X = 0, Y = 0) have a redshift and the resonance wavelengths with the input state (X = 1, Y = 1) have almost no movement. It should be noticed that when the input state is (X = 0, Y = 0), resonance wavelength has a larger redshift value than when the input states are (X = 1, Y = 0) and (X = 0,Y = 1). In other words, as the width of the rectangular resonator increases, the distance between the three wavelengths that need to be monitored increases. The above-mentioned phenomenon can be explained from the effective path of the cavity. The amount of change in the width of the rectangular resonator is denoted as D. When the input state is (X = 1, Y = 1), two sliders are moved to the right, and the change in the width of the rectangular resonator has almost no effect on the effective path of the cavity. Correspondingly, when the input states are (X = 1, Y = 0 or

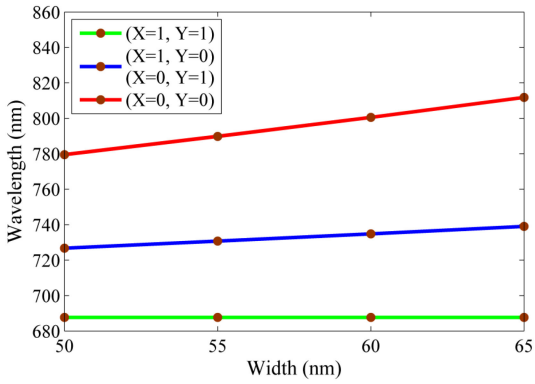

Fig. 6. Variation tendency of the resonance wavelengths as width of the rectangular resonator increases in the four input states.

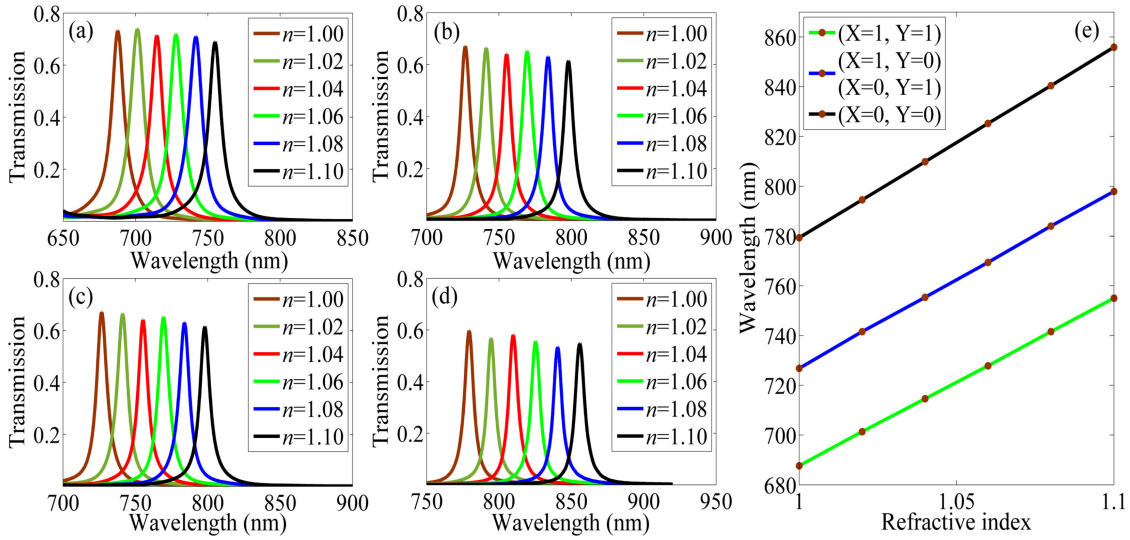

Fig. 7. The transmission spectra changes as the refractive index of the dielectric increases in (a) (X = 1, Y = 1), (b) (X = 1, Y = 0), (c) (X = 0, Y = 1), (d) (X = 0, Y = 0) states. (e) Relationship between resonance wavelength and the refractive index of the dielectric.

X = 0, Y = 1) and (X = 0, Y = 0), the variations of the effective path are $2D$ and $4D$, respectively. Therefore, During the manufacture of this device, the width of the rectangular resonator which has important effect in the transmission spectra needs to be noticed. In addition, this provides a way to change the distance of the wavelength points to be monitored.

Furthermore, we explore the relationship between the transmission characteristics and refractive index. The refractive index in the cavity increases from 1.00 to 1.10 in steps of 0.02 and the other parameters are unchanged. The transmission spectra change as the refractive index of the dielectric increases in four input states, which are shown in Figs. 7(a)–7(d). The redshift of the resonance wavelengths as the refractive index increases can be observed. As can be seen from Fig. 7(e), there is a linear relationship between them, which is consistent with the previous theoretical analysis. Therefore, we can control the resonance wavelengths by changing the refractive index of the dielectric.

4. Conclusion

In this paper, we propose a novel plasmonic logic device. It can implement three kinds of logic operations (AND, XOR and NOR) simultaneously at different wavelengths through sliding manipulation. And each logic operation can achieve a high contrast ratio, which is greater than 16 dB between the output logic states 1 and 0. In addition, we investigate the effect of structural parameters on the transmission characteristics by simulation. We can control the transmission spectra and contrast ratio by changing the structural parameter. These results provide a numerical basis for designing optical logic device. The proposed plasmonic structure may have some significance for optical computing, high-speed signal processing and highly integrated optical devices.

Acknowledgment

The authors wish to thank the anonymous reviewers for their valuable suggestions.

References

[1] W. L. Barnes, A. Dereux, and T. W. Ebbesen, "Surface plasmon subwavelength optics," *Nature*, vol. 424, no. 14, pp. 824–830, Aug. 2003.
[2] H. Lu, X. Liu, D. Mao, L. Wang, and Y. Gong, "Tunable band-pass plasmonic waveguide filters with nanodisk resonators," *Opt. Exp.*, vol. 18, no. 17, pp. 17922–17927, Aug. 2010.
[3] H. Ditlbacher, J. R. Krenn, G. Schider, A. Leitner, and F. R. Aussenegg, "Two-dimensional optics with surface plasmon polaritons," *Appl. Phys. Lett.*, vol. 81, no. 10, pp. 1762–1764, Jul. 2002.
[4] S. A. Maier and H. A. Atwater, "Plasmonics: Localization and guiding of electromagnetic energy in metal/dielectric structures," *J. Appl. Phys.*, vol. 98, no. 1, Jul. 2005, Art. no. 011101.
[5] D. K. Gramotnev and S. I. Bozhevolnyi, "Plasmonics beyond the diffraction limit," *Nature Photonics*, vol. 4, no. 2, pp. 83–91, Jan. 2010.
[6] A. Genet, and T. W. Ebbesen, "Light in tiny holes," *Nature*, vol. 445, no. 7123, pp. 39–46, Jan. 2007.
[7] S. A. Maier, "Surface plasmon polaritons at metal/insulator interfaces," in *Plasmonics: Fundamentals and Applications*, 1st ed. New York, NY, USA: Springer-Verlag, 2007, pp. 21–37.
[8] K. Wen, Y. Hu, L. Chen, J. Zhou, L. Lei, and Z. Guo, "A compact and high-efficiency dichroic plasmonic splitter based onasymmetric T-shape waveguide," *Photon. Nanostruct. Fundam. Appl.*, vol. 13, pp. 120–126, Jan. 2015.
[9] Y. Zhang and Z. Zhang, "Ultra-subwavelength and low loss in v-shaped hybrid plasmonic waveguide," *Plasmonics*, vol. 12, no. 1, pp. 59–63, Feb. 2017.
[10] A. Hosseini and Y. Massoud, "Nanoscale surface plasmon based resonator using rectangular geometry," *Appl. Phys. Lett.*, vol. 90, no. 18, Apr. 2007, Art. no. 181102.
[11] J. A. Dionne, L. A. Sweatlock, and L. A. Sweatlock, "Planar metal plasmon waveguides: Frequency-dependent dispersion, propagation, localization, and loss beyond the free electron model," *Phys. Rev. B*, vol. 72, no. 7, Aug. 2005, Art. no. 075405.
[12] X. Zhai *et al.*, "Tuning bandgap of a double-tooth-shaped MIM waveguide filter by control widths of the teeth," *J. Opt.*, vol. 15, no. 5, p. 055008, May 2013.
[13] Y. Feng *et al.*, "Compact nanofilters based on plasmonics waveguide with Archimedes spiral nanostructure," *IEEE Photon. J.*, vol. 8, no. 5, Oct. 2016, Art. no. 4802908.
[14] G. Zhan, R. Liang, H. Liang, J. Luo, and R. Zhao, "Asymmetric band-pass plasmonic nanodisk filter with mode inhibition and spectrally splitting capabilities," *Opt. Exp.*, vol. 22, no. 8, pp. 9912–9919, Apr. 2014.
[15] H. Lu, X. Liu, Y. Gong, D. Mao, and G. Wang, "Analysis of nanoplasmonic wavelength demultiplexing based on metal-insulator-metal waveguides," *J. Opt. Soc. Amer. B, Opt. Phys.*, vol. 28, no. 7, pp. 1616–1621, Jul. 2011.
[16] Y. Xie, C. He, J. Li, T. Song, Z. Zhang, and Q. Mao, "Theoretical investigation of a plasmonic demultiplexer in MIM waveguide crossing with multiple side-coupled hexagonal resonators," *IEEE Photon. J.*, vol. 8, no. 5, Oct. 2016, Art. no. 4802512.
[17] M. R. Rakhshani and M. A. Mansouri-Birjandi, "High-sensitivity plasmonic sensor based on metal–insulator–metal waveguide and hexagonal-ring cavity," *IEEE Sens. J.*, vol. 16, no. 9, pp. 3041–3046, May 2016.
[18] S. Zhang, H. Li, Z. He, B. Li, Z. Chen, and H. Xu, "Sensing analysis based on plasmon induced transparency in nanocavity-coupled waveguide," *Opt. Exp.*, vol. 23, no. 16, pp. 20313–20320, Aug. 2015.
[19] S. Yang, D. Yu, G. Liu, Q. Lin, X. Zhai, and L. Wang, "Perfect plasmon-induced absorption and its application for multi-switching in simple plasmonic system," *Plasmonics*, vol. 13, no. 3, pp. 1015–1020, Jun. 2018.
[20] Y. Zhu, X. Huang, and X. Mei, "A surface plasmon polariton electro-optic switch based on a metal-insulator-metal structure with a strip waveguide and two side-coupled cavities," *Chin. Phys. Lett.*, vol. 29, no. 6, Jun. 2012, Art. no. 064214.
[21] Y. Yu, J. Si, Y. Ning, M. Sun, and X. Deng, "Plasmonic wavelength splitter based on a metal–insulator–metal waveguide with a graded grating coupler," *Opt. Lett.*, vol. 42, no. 2, pp. 187–190, Jan. 2017.
[22] M. A. Ayad, S. S. A. Obayya, and M. A. Swillam, "Submicron 1xN ultra wideband MIM plasmonic power splitters," *J. Lightw. Technol.*, vol. 32, no. 9, pp. 1814–1820, May 2014.
[23] D. Pan, H. Wei, and H. Xu, "Optical interferometric logic gates based on metal slot waveguide network realizing whole fundamental logic operations," *Opt. Exp.*, vol. 117, no. 14, pp. 9556–9562, Apr. 2013.

[24] M. Cohen, Z. Zalevsky, and R. Shavit, "Towards integrated nanoplasmonic logic circuitry," *Nanoscale*, vol. 5, no. 12, pp. 5442–5449, May 2013.
[25] N. Nozhat, H. Alikomak, and M. Khodadadi, "All-optical XOR and NAND logic gates based on plasmonic nanoparticles," *Opt. Commun.*, vol. 392, pp. 208–213, Jun. 2017.
[26] Y. Fu, X. Hu, C. Lu, S. Yue, H. Yang, and Q. Gong, "All-optical logic gates based on nanoscale plasmonic slot waveguides," *Nano Lett.*, vol. 12, no. 11, pp. 5784–5790, Nov. 2012.
[27] N. Nozhat and N. Granpayeh, "All-optical logic gates based on nonlinear plasmonic ring resonators," *Appl. Opt.*, vol. 54, no. 26, pp. 7944–7948, May 2015.
[28] W. Zhao, D. Ju, and Y. Jiang, "Pulse controlled all-optical logic gate based on nonlinear ring resonator realizing all fundamental logic operations," *Plasmonics*, vol. 10, no. 2, pp. 311–317, Apr. 2015.
[29] Y. Ye, Y. Xie, Y. Liu, S. Wang, J. Zhang, and Y. Liu, "Design of a compact logic device based on plasmon-induced transparency," *IEEE Photon. Technol. Lett.*, vol. 29, no. 8, pp. 647–650, Apr. 2017.
[30] K. Wen, Y. Hu, L. Chen, J. Zhou, L. Lei, and Z. Guo, "Theoretical analysis of plasmonic unidirectional propagation at visible frequency based on subwavelength waveguide," *Opt. Commun.*, vol. 336, pp. 243–247, Feb. 2015.
[31] W. D. Li, W. Wu, and R. S. Williams, "Combined helium ion beam and nanoimprint lithography attains 4 nm half-pitch dense patterns," *J. Vac. Sci. Technol. B*, vol. 30, no. 6, Oct. 2012, Art. no. 06F304.
[32] T. Higashiki, T. Nakasugi, and I. Yoneda, "Nanoimprint Lithography for Semiconductor Devices and Future Patterning Innovation," *Proc. SPIE*, vol. 7970, Mar. 2011, Art. no. 797003.
[33] Y. D. Wu, "High transmission efficiency wavelength division multiplexer based on metal–insulator–metal plasmonic waveguides," *J. Lightw. Technol.*, vol. 32, no. 24, pp. 4844–4848, Dec. 2014.
[34] N. Sarkar, D. Strathearn, G. Lee, M. Olfat, and R. R. Mansour, "A platform technology for metrology, manipulation and automation at the nanoscale," in *Proc. Int. Conf. Manipulation, Automat. Robot. Small Scales*, Montreal, QC, Canada, 2017, pp. 1–6.
[35] Z. Zhang, Y. Yu, X. Liu, and X. Zhang, "Dynamic electro-thermal modeling of V- and Z-shaped electrothermal microactuator," in *Proc. IEEE Int. Conf. Mechatronics Automat.*, Harbin, China, 2016, pp. 890–895.
[36] M. Tecpoyotl-Torres, R. Cabello-Ruiz, and J. G. Vera-Dimas, "Design and simulation of an optimized electrothermal microactuator with Z-shaped beams," *Acta Universitaria*, vol. 25, no. 3, pp. 19–24, Jun. 2015.
[37] T. Hu, Y. Zhao, X. Li, Y. Zhao, and Y. Bai, "Design and fabrication of an electro-thermal linear motor with large output force and displacement," in *Proc. IEEE Sensors*, Orlando, FL, USA, 2016, pp. 1–3.
[38] J. A. Dionne, L. A. Sweatlock, and H. A. Atwater, "Plasmon slot waveguides: Towards chip-scale propagation with subwavelength-scale localization," *Phys. Rev. B*, vol. 73, no. 3, Jan. 2006, Art. no. 035407.
[39] A. Dolatabady and N. Granpayeh, "All optical logic gates based on two dimensional plasmonic waveguides with nanodisk resonators," *J. Opt. Soc. Korea*, vol. 16, no. 4, pp. 432–442, Dec. 2012.